Analyst

PAPER

View Article Online
View Journal

Cite this: DOI: 10.1039/c4an01275e

Hierarchically assembled NiCo@SiO_2@Ag magnetic core–shell microspheres as highly efficient and recyclable 3D SERS substrates†

Maofeng Zhang,[ab] Aiwu Zhao,*[ab] Dapeng Wang[a] and Henghui Sun[a]

Received 15th July 2014
Accepted 7th November 2014

DOI: 10.1039/c4an01275e

www.rsc.org/analyst

The hierarchically nanosheet-assembled NiCo@SiO_2@Ag (NSA) core–shell microspheres have been synthesized by a layer-by-layer procedure at ambient temperature. The mean particle size of NSA microspheres is about 1.7 μm, which is made up of some nanosheets with an average thickness of ~20 nm. The outer silver shell surface structures can be controlled well by adjusting the concentration of Ag^+ ions and the reaction times. The obtained NSA 3D micro/nanostructures show a structure enhanced SERS performance, which can be attributed to the special nanoscale configuration with wedge-shaped surface architecture. We find that NSA microspheres with nanosheet-assembled shell structure exhibit the highest enhancement efficiency and high SERS sensitivity to *p*-ATP and MBA molecules. We show that the detection limits for both *p*-ATP and MBA of the optimized NSA microsphere substrates can approach 10^{-7} M. And the relative standard deviation of the Raman peak maximum is ~13%, which indicates good uniformity of the substrate. In addition, the magnetic NSA microspheres with high saturation magnetization show a quick magnetic response, good recoverability and recyclability. Therefore, such NSA microspheres may have great practical potential applications in rapid and reproducible trace detection of chemical, biological and environment pollutants with a simple portable Raman instrument.

1. Introduction

Surface-enhanced Raman scattering (SERS) spectroscopy has given birth to a powerful and versatile novel analytical tool due to its high sensitivity, specificity, and fingerprint effect in the detection of analytes,[1–4] and thus has tremendous potential for chemical and biomolecular sensing and identification.[5,6] The enormous SERS enhancement effect has enabled this technique to be very sensitive which enables trace or single molecule detection of a variety of molecules, including proteins,[7] anthrax,[8] DNA,[9] explosives,[10] environmental contaminants,[11] and so on. Recently, three-dimensional (3D) Ag and Au micro/nanostructures (such as flower-like,[12] sea urchin-like,[13,14] star-like,[15] sphere-like,[16] as well as dendritic morphologies[17]), which contain special fine structure, large specific surface area, and larger size, have stimulated great interest for several obvious advantages and their excellent performance as SERS substrates. Both experimental measurements and theoretical calculations have proven that strong electromagnetic field enhancement can be produced between adjacent nanostructures on the surface of the 3D complex structures.[18–20] To date, various kinds of 3D Ag and Au micro/nanostructures have been successively synthesized and reported. Despite these amazing advances, it must be emphasized that most of these SERS substrates are thrown away after one detection probably because they cannot be recycled. This would result in a waste of the resources which usually are made of noble metals (Au or Ag). From the application viewpoint, it is of considerable importance to develop an efficient SERS substrate that can not only provide strong enhancement factors, but also show high stability and reproducibility.

The combination of noble metals and magnetic materials as SERS substrates has been proved to be an effective way of solving the problem described above. Magnetic-based noble metal composites can be recycled, are economical, and their function can be recovered by several washing steps. In particular, the combination of plasmonic and magnetic materials in a single micro/nanostructure is of high interest to the biomedical community because it has the potential to lead to new biological applications, such as immunomagnetic separation under plasmonic imaging monitoring, dual mode imaging (MRI and plasmonic imaging), and SERS sensing. For example, Yang *et al.* had demonstrated the synthesis of Ag-coated Fe_3O_4 microspheres as a SERS substrate holding clean and reproducible properties under an external magnetic force.[21] Also, they showed a facile one-step solvothermal method for the synthesis

[a]Institute of Intelligent Machines, Chinese Academy of Sciences, Hefei, 230031, P. R. China. E-mail: awzhao@iim.ac.cn

[b]State Key Laboratory of Transducer Technology, Chinese Academy of Sciences, Hefei, 230031, P. R. China

† Electronic supplementary information (ESI) available. See DOI: 10.1039/c4an01275e

of sea-urchin-like Fe_3O_4@C@Ag particles, which can be used as a SERS substrate possessing reproducible properties;[22] Wang *et al.* reported a well-dispersed Fe_3O_4@SiO_2@Ag with a nanosheet assembled shell structure exhibiting good reproducibility across the entire area;[23] recently, our group has developed Fe_3O_4@C@Au composite microspheres with superior SERS detection and recyclable catalytic degradation abilities for organic dyes.[24] The above-mentioned magnetic core–shell materials generally employ Fe_3O_4 as a magnetic core, while metals and alloy materials (such as Fe, Co, Ni, FePt, and FePd) are less commonly employed as magnetic cores,[25] in part because of their rapid oxidation in air and/or potential of cytotoxicity. Importantly, these metals and alloy materials are specifically appealing because they often possess high saturation magnetization which means that they are easy to be separated, recycled and renewed through an external magnet. To overcome these drawbacks, a silica or carbon shell is introduced on the magnetic core to provide protection against oxidation, cytotoxicity and help to maintain long-term stability of the particles.[26,27]

Thus, it is of great importance to develop a facile and effective method for the synthesis of metal and alloy based noble metal composite structures and exploring their SERS and reproducible performance. Unfortunately, there are few reports on the synthesis and SERS performance of metal and alloy based silver composite microspheres to date. In this paper, we report a new route to fabricate monodispersed NiCo@SiO_2@Ag (NSA) composite microspheres with an ideal reproducible nanosheet-assembled shell structure from which strong SERS signals can be generated. The NSA composite microspheres were synthesized in three main steps based on a layer-by-layer procedure. Firstly, the magnetic NiCo alloy spheres as the core were prepared by a solution reaction at room temperature. Secondly, the NiCo alloy spheres were coated with a layer of silica by a modified Stöber method, which would disperse them well in water due to the hydrophilic properties of the silica shell. Thirdly, Ag seeds were introduced onto the surface of the silica shell for easier deposition of the subsequent silver shell, and then the Ag nanosheet-assembled shell was successfully formed around the NiCo@SiO_2 microspheres. Raman experiments indicated that NSA composite microspheres with nanosheet-assembled shell structure showed the highest enhancement efficiency and high SERS sensitivity to *p*-aminothiophenol (*p*-ATP) and 4-mercaptobenzoic acid (MBA) molecules. And a low concentration of 10^{-7} M for both *p*-ATP and MBA could be detected. Such NSA composite microspheres exhibited good reproducibility across the entire area. Moreover, the superiority of the NSA composite microspheres in terms of their recoverability and recyclability was demonstrated through many successive cycles, under the external magnetic field.

2. Experimental section

2.1. Sample preparation

Synthesis of NSA composite microspheres. NSA composite microspheres were prepared according to the previous method with minor modification.[23] 50 mg of the obtained NiCo@SiO_2 microspheres were first ultrasonically dispersed in 20 mL of absolute ethanol for 30 min, then mixed with $[Ag(NH_3)_2]^+$ solution (2 mmol $AgNO_3$, 2 mL $NH_3 \cdot H_2O$, 20 mL ethanol) and stirred for 300 min. After separation by a magnet, 40 mL of ethanol containing 0.2 g of PVP was added, and the mixed solution was kept in a sealed flask at 70 °C under vigorous mechanical stirring and occasional sonication. After 3 h, NSA seed microspheres were obtained. Then, the above-obtained NSA seed microspheres were redispersed in a mixed solution containing 2 mL $AgNO_3$ (0.5 M), 0.2 g citrate acid, and 40 mL deionized water under sonication and a mechanical stirrer, and then an ascorbic acid solution (0.1 g, 10 mL) was added drop by drop in 15 minutes, and the reaction process was conducted under mechanical stirring and sonication. After the reaction was completed, the sample was washed with ethanol and deionized water repeatedly. Finally, the products were redispersed in 1 mL ethanol for further characterization.

2.2. Characterization

Field emission scanning electron microscope images were taken with a field emission scanning electron microscope (Quanta 200 FEG) operated at an accelerating voltage of 10.0 kV (ZYVEX, America). Transmission electron microscopy (TEM) and selected area electron diffraction (SAED) studies were performed with a JEOL-2010 microscope operated at an accelerating voltage of 200 kV with a tungsten filament. The phase and composition of the products were determined by a Rigaku D/Max-γA rotating-anode X-ray diffractometer equipped with monochromatic high-intensity Cu-Kα radiation ($\lambda = 1.54187$ Å). The magnetic characterization of the samples was performed by using a superconducting quantum interference device (SQUID, Quantum Design MPMS-XL) magnetometer with fields up to 20 000 Oe. All measurements were performed at room temperature. The UV-Vis absorption spectra of the samples were recorded with a Shimadzu DUV-3700 spectrophotometer.

2.3. SERS measurement

p-ATP and MBA molecules were used as a Raman probe for the SERS measurements. For preparation of SERS substrates, the as-prepared NSA composite microspheres were immersed in 0.2 mL of *p*-ATP and MBA ethanol solutions respectively, then the samples were extracted using an external magnet and washed with ethanol and deionized water, and dried in air before the subsequent characterization. After the sample was carefully dropped onto clean glass slides, the substrates were measured using a Raman instrument. All SERS and Raman spectra were collected by a portable Raman instrument (*i*-Raman, B&W Tek Inc., USA) attached with a microscope (20× objective) and an optical fiber. The laser excitation wavelength was 1064 nm. During SERS measurements, the laser light was vertically projected onto the samples, and all SERS spectra were recorded by focusing the laser on the surface of the samples with a total accumulation time of 5 s. For each substrate, we took three SERS spectra at different positions of the substrate and then averaged them.

3. Results and discussion

3.1. Morphology and structure of the sample

Preparation of NSA microspheres involves three main steps: Fabrication of magnetic NiCo particles as the core, coating silica onto the NiCo particles, and Ag nanosheet-assembling around the NiCo@SiO_2 microspheres. The typical SEM and TEM images in Fig. 1A–C show that uniform and monodispersed spherical particles with textured surface structure and a diameter of about 1.3 μm can be obtained using this method. Fig. 1D–F present the images of uniform NiCo@SiO_2 microspheres with a core–shell structure. The silica shell is clearly visible as shown in Fig. 1F. Moreover, the shell thickness can be controlled by varying the concentration of TEOS and the reaction time.[28] The silica shell thickness of about 60 nm is controllably synthesized for the following assembling of the silver shell. In this work, the silica shell on the NiCo core not only effectively provides protection against oxidation and cytotoxicity, but also improves the dispersibility of the magnetic microspheres. Fig. 1G–I show images of Ag nanosheets assembled around NiCo@SiO_2 microspheres obtained under sonication and mechanical stirring conditions. They clearly reveal that large quantity and good uniformity of NSA microspheres with a mean particle size of about 1.7 μm are achieved using this approach (Fig. 1G), which are much bigger than those of NiCo@SiO_2 microspheres, and the thickness of the Ag shell was estimated to be around 350 nm. It is also clear from Fig. 1H that as-obtained microspheres have a hierarchical surface structure which is assembled from many nanosheets with a thickness of about 20 nm. These nanosheets entangle with each other and form a wedge-shaped surface architecture. Rough edges are also seen around the composite microspheres in the TEM image in Fig. 1I. Both the SEM and TEM images indicate that we have succeeded in controllable synthesis of spherical NSA core–shell micro/nanostructures.

A partial surface of a hierarchical NSA microsphere is shown in Fig. 2A, which indicates that the nanosheets self-assembled into a spherical structure. The TEM image of a single NSA microsphere exhibits regions of varying contrast from the cores to the edges (Fig. 2B). The thin nanosheets are observed clearly at the edge of the microsphere. The HRTEM image (Fig. 2C) shows that the nanosheets are single-crystalline protrusions with an interplanar spacing of about 0.245 nm. The SAED pattern (the inset in Fig. 2C) taken from this nanosheet reveals the hexagonal spot arrays which can be assigned to the [$\bar{1}11$] orientation of the FCC structure. The X-ray diffraction (XRD) patterns of the magnetic particles are displayed in Fig. 2D. The pattern (Fig. 2D(a)) can be easily indexed to NiCo alloys. The diffraction peaks (Fig. 2D(b)) of the NSA microspheres can be assigned to the (111), (200), and (220) planes of silver, respectively. The sharp and intense diffraction peaks of the NSA microspheres indicate high crystallinity of the particles. All the diffraction peaks of the products can be easily indexed to a cubic phase [space group $Fm\bar{3}m$] of silver (PDF no. 04-0783).

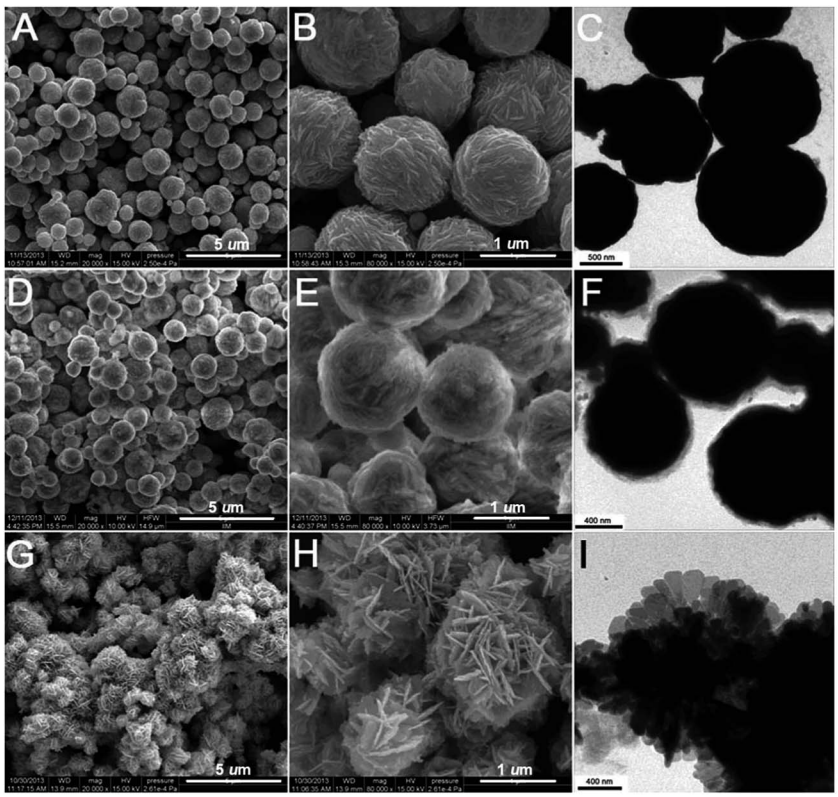

Fig. 1 SEM images of (A) NiCo, (D) NiCo@SiO_2, and (G) NSA microspheres, and their corresponding magnified SEM images (B, E, and H), and TEM images (C, F, and I), respectively.

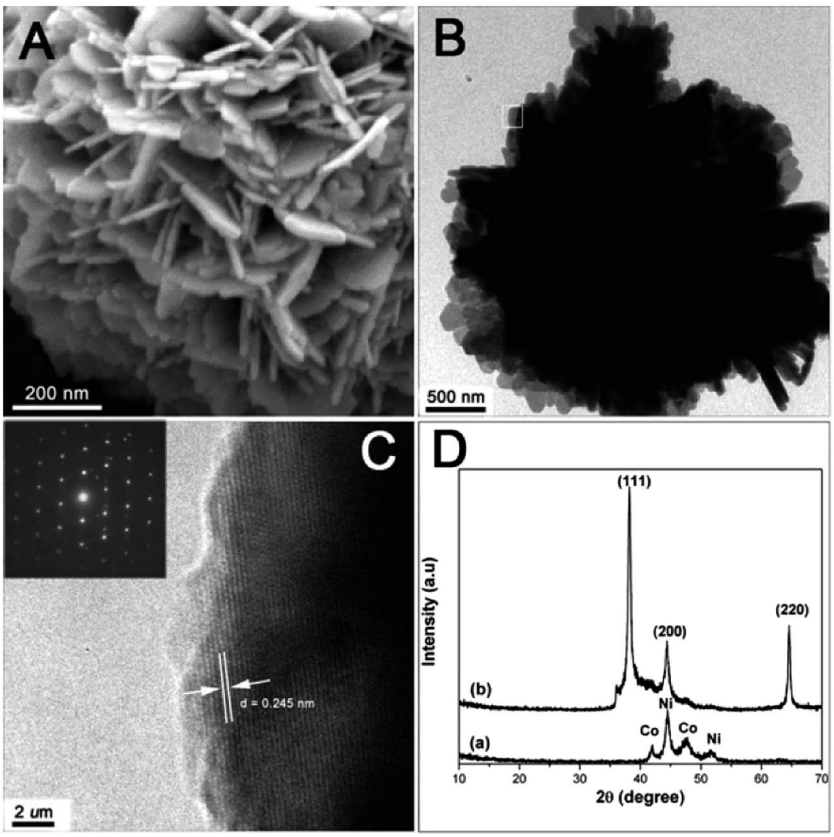

Fig. 2 Representative SEM image of (A) partial surface of NSA microsphere; (B) TEM image of a single NSA microsphere; (C) HRTEM image of a single Ag nanosheet and the SAED pattern (the inset) taken from the white square in (B); and (D) XRD patterns of the as-prepared (a) NiCo particles and (b) NSA microsphere.

Besides, no obvious sharp diffraction peak corresponding to the SiO_2 is present, indicating that the SiO_2 coated around NiCo is amorphous. The increasing intensity of sharp diffraction peaks from the NSA microspheres shields the intensity of that from the NiCo, which indirectly proves the gradual growth of a silver shell around the NiCo@SiO_2 microspheres.

3.2. The evolution of the morphology and surface structure of the products

In the silver shell coating process, the silver seed modification has proved to be an efficient method for increasing the degree of surface coverage, since direct coating of a silver shell is rather difficult.[29] In order to introduce Ag seeds into the composites, NiCo@SiO_2 microspheres were first immersed into a $[Ag(NH_3)_2]^+$ solution for attraction and accumulation of some silver ions on the silica surface. Subsequently, Ag seeds were grown onto the surface of NiCo@SiO_2 microspheres through reduction of Ag ions by PVP in ethanol (Fig. 3A). These small silver nanoparticles served as nuclei sites for the subsequent growth of silver shells. The products synthesized at different reaction intervals were sampled and observed by SEM. During the silver shell growth, ascorbic acid (AA) was used as a reductant. After reaction for 2 min, the original spherical NSA particles were produced (Fig. 3B), revealing that the initial silver seeds successfully played the role of growing nuclei. With

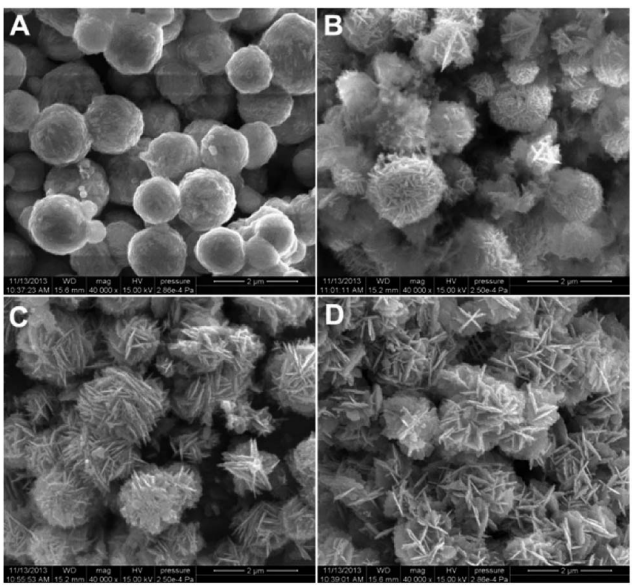

Fig. 3 The SEM images of NSA microspheres synthesized with $AgNO_3$ (2 mL) for different growing stages: (a) seeding, (b) 2 min, (c) 5 min and (d) 15 min respectively.

further extension of the reaction time to 5 min, the products grew bigger with the addition of AA and many dense nanosheets assembled on the surface of the products can be observed

(Fig. 3C). On further increase in reaction time to 15 min, a complete Ag shell with rough edges on the surface of NiCo@SiO_2 microspheres was formed (Fig. 3D). To obtain well-dispersed NSA microspheres, we carried out the coating experiments under the mechanical stirring and using the sonication technique, together with the dropwise addition of a reducer.

Further experiments have revealed that the concentrations of $AgNO_3$ also affect the final silver unit's morphology in our experiments. Tuning the concentrations of $AgNO_3$ from 4 mL to 0.5 mL resulted in different surface features of the products while the general morphology of microspheres remained almost unchanged. In these cases, the amount of citrate ions which is one kind of a morphology controlling reagent was kept constant. For example, when the amount of $AgNO_3$ was increased to 4 mL, NSA microspheres with thicker sheets (~80 nm) were obtained (Fig. 4A and B). Decreasing the amount of $AgNO_3$ to 2 mL resulted in the formation of thin nanosheet (20 nm) assembled NSA microspheres as displayed in Fig. 4C and D. With the decrease of $AgNO_3$ to 1 mL, the NiCo@SiO_2 microspheres were covered by short Ag nanosheets (Fig. 4E and F). However, with further decrease of $AgNO_3$ to 0.5 mL, sparse and shorter Ag nanosheet assembled NSA microspheres were produced as shown in Fig. 4G and H. Because of the insufficient amount of $AgNO_3$, some parts of the NiCo@SiO_2 surface were exposed outside. It is reported that citrate ions not only serve as a capping agent to selectively bind {111} facets, but also coordinate with Ag^+ ions to form a variety of complexes. The coordination effect can significantly reduce the concentration of free Ag^+ ions, thus slowing down the reduction and enabling a kinetic control that favors nanoplate formation.[30] In our experiment, when a large amount of $AgNO_3$ was adopted (for example, 4 mL), although a half of the silver ions were proposed to be complexed with citrate ions in solution, the concentration of free Ag^+ ions increased largely. Then, thermodynamic growth began to work, and the citrate ions attached onto the {111} facets of silver units could not strongly restrict the growth along the planar directions; thus the gradual growth along the vertical directions led to the thicker nanosheets seen in Fig. 4B. When the amount of $AgNO_3$ was decreased from 2 mL to 0.5 mL, citrate ions could completely stabilize the silver ions, favoring the growth of nanosheets.

3.3. The magnetic response of the products

In the present work, the NSA composite microspheres could simultaneously attain dual functions of both fast magnetic response and local surface plasmon resonance. The magnetic properties of the NiCo microspheres and NSA microspheres were first characterized by a SQUID magnetometer at room temperature. As shown in Fig. 5, the saturation magnetization (Ms) values of NiCo microspheres and NSA microspheres are about 175 emu g^{-1} and 43 emu g^{-1}, respectively. Such an excellent magnetic property means that all of the prepared

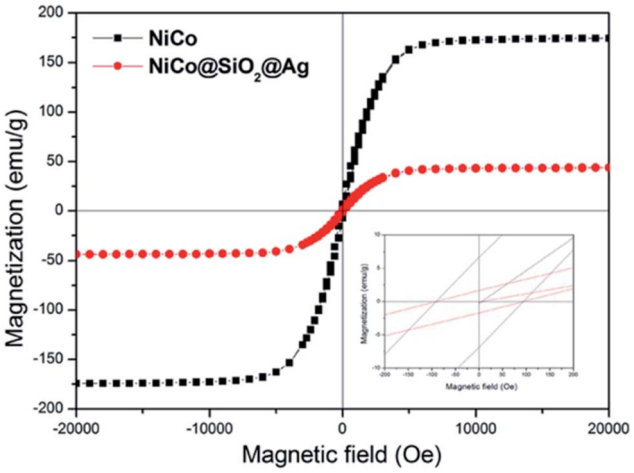

Fig. 5 Magnetic hysteresis loops of the NiCo microspheres and NSA composite microspheres (the inset shows the magnified low field curves).

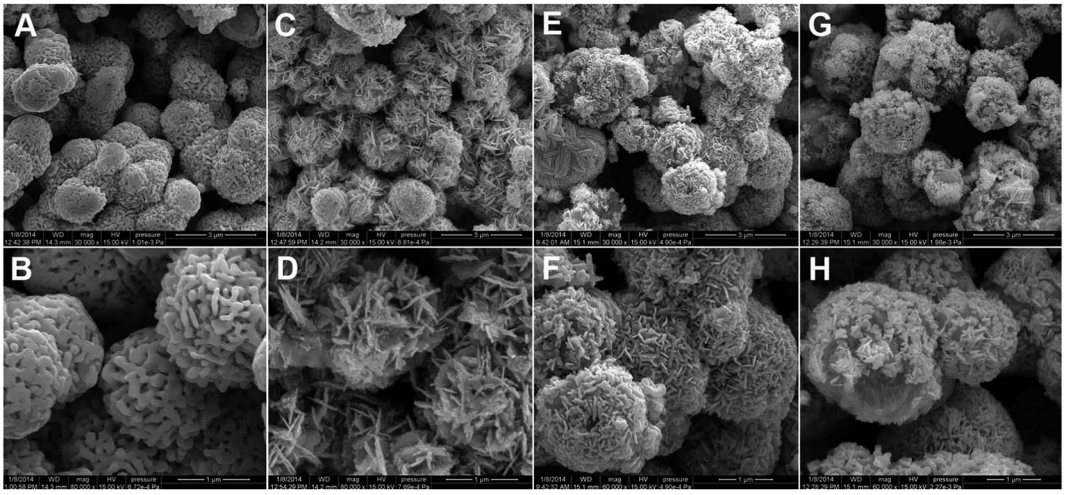

Fig. 4 The SEM images of NSA composite microspheres synthesized with different concentrations of $AgNO_3$: (A) 4 mL, (C) 2 mL, (E) 1 mL and (G) 0.5 mL, and their corresponding magnified SEM images (B, D, F and H).

samples have strong magnetic responsivity and hence can be separated easily from solution with the help of an external magnetic force and can be used for recyclable application. The sharp decrease in magnetic saturation can be explained in terms of the formation of the SiO_2 and Ag shell surrounding the NiCo microspheres.[37] The magnified low field curves also demonstrate the minor magnetic hysteresis loops of the NiCo microspheres and NSA microspheres (the inset in Fig. 5). Moreover, the suspensions of both the NiCo microspheres and NSA microspheres can be concentrated by an external magnet within 30 s, leaving the aqueous solution transparent. When the magnet was removed, the NSA microspheres were well dispersed again in the aqueous solution by shaking, demonstrating that the NSA microspheres have a good water-dispersive ability. When these NSA microspheres are used as Raman probes, analyte molecules can be easily captured, magnetically concentrated, and analyzed by SERS. Compared with pure silver microspheres, the obtained magnetic-based hierarchical silver microspheres can be separated from the sample solution, which shortens the detecting time. Moreover, the rapid magnetic response ability allows for the tracking or separation of such particles in a magnetic gradient, paving the way for their sensitive and recyclable detection of probe molecules.

3.4. Reproducible SERS substrate for high sensitivity detection

It is well known that SERS spectroscopy is a unique ultrasensitive technique that allows identification of the analytes. The presence of cross-linked nanosheets assembled around $NiCo@SiO_2$ microspheres is expected to significantly promote local field enhancements on the surface of these particles that might increase their SERS efficiency. Using a portable Raman spectrometer, our SERS platform can identify *p*-ATP molecules. Fig. 6A shows the SERS spectra of *p*-ATP adsorbed on NSA microsphere substrates prepared at different reaction intervals. The primary vibrations of *p*-ATP are confirmed according to our previous work[31] and the literature.[32,33] Two sets of bands were observed in the SERS spectra of *p*-ATP on the surface of NSA microspheres. One set is located at 1073 and 1587 cm^{-1}, which is assigned to the a_1 vibrational modes and the other set is located at 1136 and 1440 cm^{-1}, which is assigned to the b_2 vibrational modes. Obviously, the SERS intensity of the NSA seed microspheres is the lowest, since only some tiny silver nanoparticles were decorated on the surface of the $NiCo@SiO_2$ microspheres. The SERS intensity increases with the increase of coating time and reaches a maximal value for 15 min. The reason can be explained by the fact that the content of silver and the number of silver nanosheets increase with prolonged coating time which leads to formation of a large number of gaps or voids, providing more active sites which afford potential high density 'hot spots' to amplify the local electromagnetic fields as well as the Raman signal. In addition, the SERS performance of products with different morphologies shown in Fig. 4B–H was also investigated. From Fig. 6B, it is observed that the roughened NSA microspheres with cross-linked thin nanosheets (Fig. 4D) showed the best SERS performance compared with the other shapes. This result can be explained in two aspects. Firstly, the NSA microspheres with cross-linked thin nanosheets (Fig. 4D) showed the strongest plasmon peak at around 356 nm compared with the other morphologies (shown in Fig. S2†). When excited by the irradiation, it could give rise to the strongest SERS performance. Secondly, the reason was proposed to be the different morphologies of the shell. It is widely believed that a large enhancement could occur when a SERS active molecule is positioned within the gap between two closely spaced metallic nanostructures.[37] The nano-scale cracks between two neighbouring nanosheets seen in Fig. 2A were also proposed to contribute to the SERS enhancement. And it was found the SERS signals weakened with decreasing density of nanosheets in Fig. 4H, due to the lower density of nanogaps providing fewer "hot spots" around the surface, thus resulting in inferior SERS signals.

In this study, the sensitive properties of the NSA composite microspheres with maximum enhancement efficiency were selected as SERS substrates to detect representative SERS-active analytes such as *p*-ATP and MBA to test their effects. Fig. 7a demonstrates the results of SERS spectra of *p*-ATP with different concentrations adsorbed on the substrate from 10^{-4} M to 10^{-7}

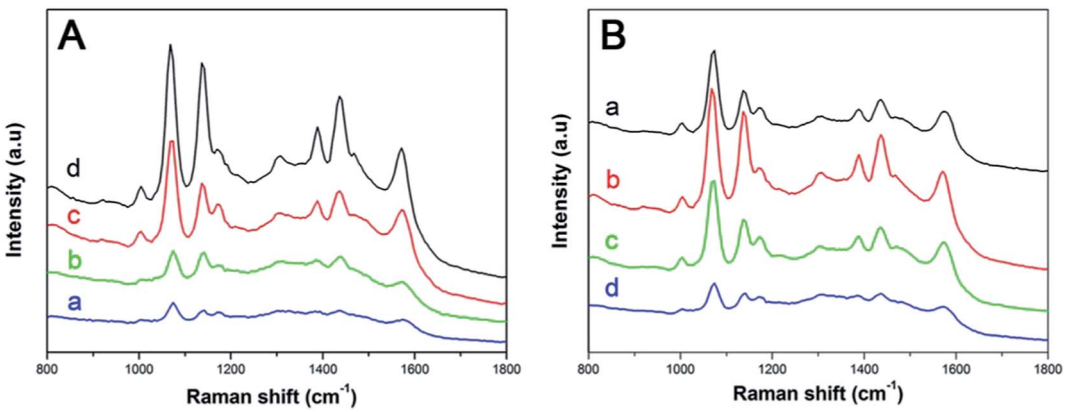

Fig. 6 SERS spectra of *p*-ATP (10^{-5} M) adsorbed on NSA composite microspheres (A) synthesized at different growing stages: (a) seeding, (b) 2 min, (c) 5 min and (d) 15 min; (B) with different morphologies shown in (a) Fig. 4B, (b) Fig. 4D, (c) Fig. 4F, and (d) Fig. 4H.

M. All the peaks observed in our SERS spectra can be attributed to *p*-ATP. The spectral intensities and resolutions are decreased by diluting the concentrations of the target molecules. It is found that additional *p*-ATP peaks still appeared at about 1073 and 1587 cm^{-1} at a low concentration of 10^{-7} M, which indicates that this SERS substrate is highly sensitive and promising for the detection of other target molecules. Hence, we examined the detection sensitivity of the as-obtained NSA composite microspheres for the detection of MBA molecules. The SERS spectra of MBA with different concentrations adsorbed on the NSA composite microsphere substrate are shown in Fig. 7b. The peaks from 800 to 1800 cm^{-1} are attributed to MBA signals; the two strong SERS peaks appearing at 1073 and 1582 cm^{-1} are assigned to ν_{8a} and ν_{12} aromatic ring vibrations, respectively; other weak bands around 1147 and 1181 cm^{-1} are attributed to the C–H deformation modes.[34] It is observed that two obvious SERS bands can still be detected in concentration ranges down to 10^{-7} M. This result indicated that a NSA composite microsphere substrate also exhibited high detection sensitivity for MBA. In order to observe the enhancement intuitively and quantitatively, the SERS enhancement factor (EF)[35] was calculated as follows:

$$\mathrm{EF} = \frac{I_{\mathrm{SERS}}/N_{\mathrm{SERS}}}{I_{\mathrm{bulk}}/N_{\mathrm{bulk}}}$$

where I_{SERS} and I_{bulk} denote the Raman scattering intensities from the *p*-ATP adsorbed on the surface of NSA composite microspheres and the solid *p*-ATP, respectively. N_{SERS} and N_{bulk} represent the numbers of the corresponding surface and solid molecules effectively excited by the laser beam, respectively. Based on the Raman intensity of the a_1 vibrational modes at 1073 cm^{-1} and b_2 vibrational modes at 1175 cm^{-1} (Fig. S1, ESI†), the EF for a_1 and b_2 vibrational modes were calculated to be 3.0×10^5 and 4.8×10^5, respectively, also showing good SERS activity of the NSA composite microsphere substrate. The uniformity of the NSA substrate was evaluated by collecting *p*-ATP (10^{-6} M) SERS spectra at 50 points that were randomly chosen on the substrate, and the relative standard deviations (RSD) of the intensities of the main vibrations were calculated, as shown in Fig. 8, respectively. Above all, the main Raman vibrations of *p*-ATP were obviously enhanced to a different extent at all spots of the NSA microsphere substrate, while the values of the RSD for the vibrations at 1073, 1136 and 1587 cm^{-1} are 11.27, 9.50, and 12.09%, respectively, which are consistently less than 13%, further indicating the uniformity of the substrate.[36,37]

Based on the above analysis, it is clear that the Ag nanosheet-assembled NSA composite microspheres achieve high enhancement efficiency. Several factors are believed to simultaneously contribute to the Raman enhancement. The nanoscale gaps between neighbouring nanosheets on the surface of NSA provide high density hot spots, and the close approach of two entangled Ag nanosheets led to interaction of their localized surface plasmon resonances (LSPR), which is beneficial for SERS activity.[38,39] When excited by the incident radiation, a collective surface plasmon is trapped between the neighbouring nanoscale gaps, thus creating a huge local electric field at these gaps. Also their rough surface possesses a high specific surface area which favors the adsorption of probing molecules and the formation of high density and uniform gaps is easy for NSA to trap and capture probing molecules. Thus, it is not surprising that the NSA as a SERS substrate performed with distinguished sensitivity and uniformity.

Finally, the recyclability of the substrate was examined through a series of experiments. A renewable substrate can be obtained for further detection if the target molecules adsorbed on the substrate can be fully cleaned by simple washing using water or ethanol. Fig. 9 shows the reversible SERS behavior of *p*-ATP and MBA adsorbed on the NSA microspheres over three cycles. By a simple magnetic separation, the substrate could be reused three times with no obvious decrease of the SERS intensity. The main reason for losing SERS signals is that the adsorbed target molecules on the substrate are washed away. Obviously, it is very simple and easy to realize the cleaning goal since the amount of target molecules adsorbing onto the substrate is low. After the substrate becomes clean, it can be repeatedly used several times. The SERS intensity does not show any obvious loss after three recycles for the detection of *p*-ATP or MBA. It is well-known that magnetic separation renders the recovery of material from a liquid reaction system much easier than the traditional separation procedures, such as filtration and centrifugation. The strong magnetic responsivity of NSA

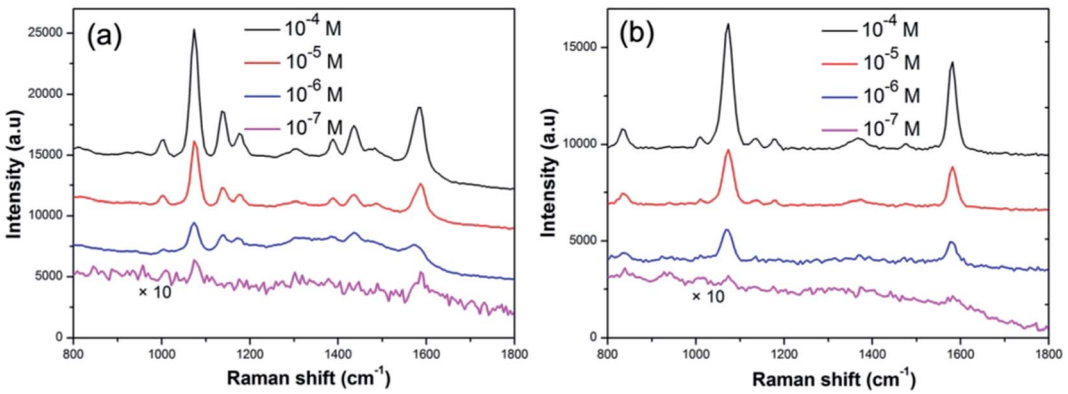

Fig. 7 SERS spectra obtained from different concentrations of (a) *p*-ATP and (b) MBA adsorbed on NSA composite microspheres.

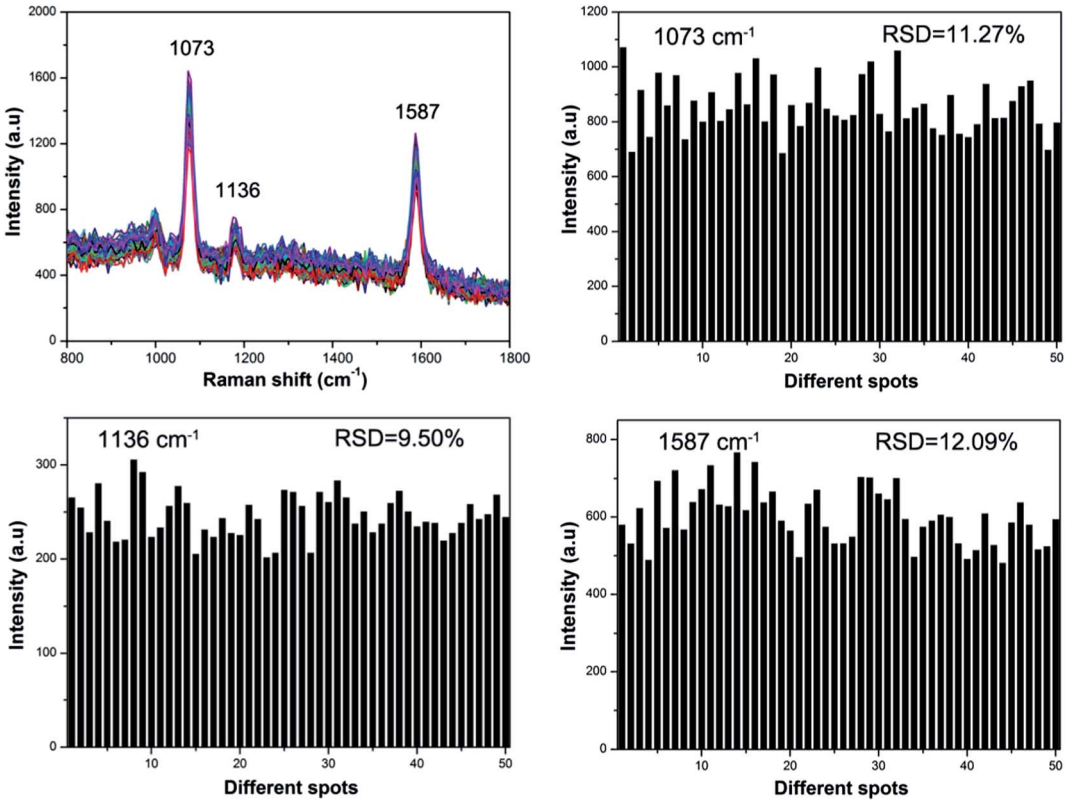

Fig. 8 A series of SERS spectra of *p*-ATP (10^{-6} M) molecules collected on 50 randomly selected spots of the NSA microspheres, and the intensities of the main Raman vibrations of *p*-ATP for SERS line-scan spectra collected on the NSA microspheres.

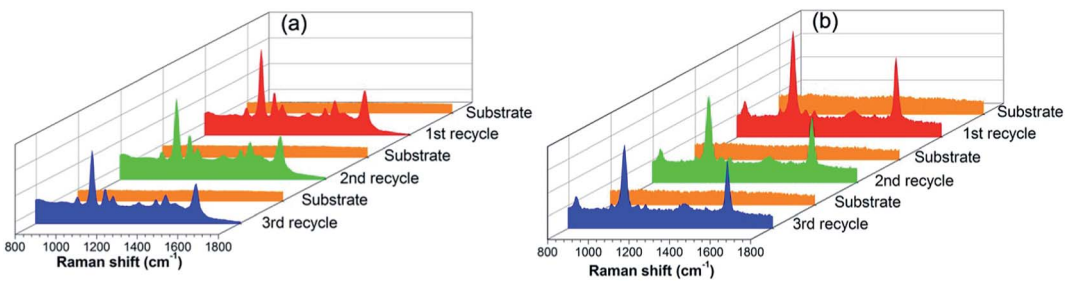

Fig. 9 Reversible SERS behavior of (a) 10^{-6} M *p*-ATP and (b) 10^{-6} M MBA on the NSA microspheres over three cycles.

microspheres (Fig. 5) is satisfied with the separation and collection in this study. This will provide an easy and efficient way to separate and recycle NSA microspheres from a suspension system with the help of an external magnetic force.

4. Conclusions

In summary, 3D hierarchically nanosheet-assembled NiCo@SiO_2@Ag composite microspheres have been successfully prepared by a layer-by-layer procedure at ambient temperature. The different surface structure of the silver shell can be obtained and controlled by adjusting the concentration of $AgNO_3$ and the reaction times. The gaps in or between cross-linked nanosheets in the shell of the microspheres are proposed to provide sufficient "hot spots" when they are used as a SERS substrate. The SERS measurement results, which are performed using a portable Raman instrument equipped with an optical fiber, show that NSA microspheres with nanosheet-assembled shell structure exhibit the highest enhancement efficiency and high SERS sensitivity to *p*-aminothiophenol (*p*-ATP) and 4-mercaptobenzoic acid (MBA) molecules. The resulting SERS substrate showed a highest analytical enhancement factor of $\sim 10^5$, a detection limit $\sim 10^{-7}$ M and a relative standard deviation of the Raman peak maximum of ~13%. In addition, the NSA microspheres with high saturation magnetization exhibit a quick response to an external magnetic field and show a good recoverability and recyclability. This research has great practical potential applications in rapid, on-site and reproducible trace detection of chemical, biological and hazardous materials in the field.

Acknowledgements

This work was supported by the National Natural Science Foundation of China (no. 61205150 and no. 61378038) and the State Key Laboratories of Transducer Technology.

Notes and references

1 X. H. Xia, J. Zeng, B. McDearmon, Y. Q. Zheng, Q. G. Li and Y. N. Xia, *Angew. Chem., Int. Ed.*, 2011, **50**, 12542–12546.
2 G. Sinha, L. E. Depero and I. Alessandri, *ACS Appl. Mater. Interfaces*, 2011, **3**(7), 2557–2563.
3 Z. Liu, L. Cheng, L. Zhang, C. Jing, X. Shi, Z. B. Yang, Y. T. Long and J. X. Fang, *Nanoscale*, 2014, **6**, 2567–2572.
4 M. Liu, Z. Y. Wang, S. F. Zong, H. Chen, D. Zhu, L. Wu, G. H. Hu and Y. P. Cui, *ACS Appl. Mater. Interfaces*, 2014, **6**(10), 7371–7379.
5 J. F. Li, Y. F. Huang, Y. Ding, Z. L. Yang, S. B. Li, X. S. Zhou, F. R. Fan, W. Zhang, Z. Y. Zhou, D. Y. Wu, B. Ren, Z. L. Wang and Z. Q. Tian, *Nature*, 2010, **464**, 392–395.
6 C. M. Girish, S. Iyer, K. Thankappan, V. V. Divya Rani, G. Siddaramana Gowd, D. Menon, S. Nair and M. Koyakutty, *J. Mater. Chem. B*, 2014, **2**, 989–998.
7 X. M. Kong, Q. Yu, X. F. Zhang, X. Z. Du, H. Gong and H. Jiang, *J. Mater. Chem.*, 2012, **22**, 7767–7774.
8 K. Ryu, A. J. Haes, H. Y. Park, S. Nah, J. Kim, H. Chung, M. Y. Yoon and S. H. Han, *J. Raman Spectrosc.*, 2010, **41**, 121–124.
9 M. Li, S. K. Cushing, H. Y. Liang, S. Suri, D. L. Ma and N. Q. Wu, *Anal. Chem.*, 2013, **85**, 2072–2078.
10 A. Chou, E. Jaatinen, R. Buividas, G. Seniutinas, S. Juodkazis, E. L. Izake and P. M. Fredericks, *Nanoscale*, 2012, **4**, 7419–7424.
11 Y. Zhou, J. Chen, L. Zhang and L. B. Yang, *Eur. J. Inorg. Chem.*, 2012, 3176–3182.
12 M. F. Zhang, A. W. Zhao, H. H. Sun, H. Y. Guo, D. P. Wang, D. Li, Z. B. Gan and W. Y. Tao, *J. Mater. Chem.*, 2011, **21**, 18817–18824.
13 X. S. Wang, D. P. Yang, P. Huang, M. Li, C. Li, D. Chen and D. X. Cui, *Nanoscale*, 2012, **4**, 7766–7772.
14 R. Li, C. Han and Q. W. Chen, *RSC Adv.*, 2013, **3**, 11715–11722.
15 W. Moukarzel, J. Fitremann and J. Marty, *Nanoscale*, 2011, **3**, 3285–3290.
16 H. Wei, B. Li, Y. Du, S. Dong and E. Wang, *Chem. Mater.*, 2007, **19**, 2987–2993.
17 Y. Qin, Y. Song, N. Sun, N. Zhao, M. Li and L. Qi, *Chem. Mater.*, 2008, **20**, 3965–3972.
18 J. F. Li, Y. F. Huang, Y. Ding and Z. L. Yang, *Nature*, 2010, **464**, 392–395.
19 H. Wang and N. J. Halas, *Adv. Mater.*, 2008, **20**, 820–825.
20 P. S. Kumar, I. Pastoriza-Santos, B. Rodriguez-Gonzalez, F. J. Garcia de Abajo and L. M. Liz-Marzan, *Nanotechnology*, 2008, **19**, 1–5.
21 L. B. Yang, Z. Y. Bao, Y. C. Wu and J. H. Liu, *J. Raman Spectrosc.*, 2012, **43**, 848–856.
22 Y. J. Ye, J. Chen, Q. Q. Ding, D. Y. Lin, R. L. Dong, L. B. Yang and J. H. Liu, *Nanoscale*, 2013, **5**, 5887–5895.
23 Y. Q. Wang, K. Wang, B. F. Zou, T. Gao, X. L. Zhang, Z. L. Du and S. M. Zhou, *J. Mater. Chem. C*, 2013, **1**, 2441–2447.
24 Z. B. Gan, A. W. Zhao, M. F. Zhang, W. Y. Tao, H. Y. Guo, Q. Gao, R. R. Mao and E. H. Liu, *Dalton Trans.*, 2013, 8597–8605.
25 N. T. T. Trang, T. T. Thuy, K. Higashimine, D. M. Mott and S. Maenosono, *Plasmonics*, 2013, **8**(2), 1177–1184.
26 B. L. Cushing, V. L. Kolesnichenko and C. J. O'Connor, *Chem. Rev.*, 2004, **104**, 3893–3946.
27 L. X. Zhang, X. P. Sun, Y. H. Song, X. Jiang, S. J. Dong and E. A. Wang, *Langmuir*, 2006, **22**, 2838–2843.
28 M. Ohmori and E. Matijevic, *J. Colloid Interface Sci.*, 1993, **160**, 288–292.
29 J. H. Zhang, J. B. Liu, S. Z. Wang, P. Zhan, Z. L. Wang and N. B. Ming, *Adv. Funct. Mater.*, 2004, **14**, 1089–1096.
30 J. Zeng, J. Tao, W. Y. Li, J. Grant, P. Wang, Y. M. Zhu and Y. N. Xia, *Chem.–Asian J.*, 2011, **6**, 376–379.
31 M. F. Zhang, A. W. Zhao, D. Li, H. H. Sun, D. P. Wang, H. Y. Guo, Q. Gao, Z. B. Gan and W. Y. Tao, *RSC Adv.*, 2014, **4**, 9205–9212.
32 Q. Zhou, G. Zhao, Y. W. Chao, Y. Li, Y. Wu and J. W. Zheng, *J. Phys. Chem. C*, 2007, **111**, 1951–1954.
33 Y. F. Huang, D. Y. Wu, H. P. Zhu, L. B. Zhao, G. K. Liu, B. Ren and Z. Q. Tian, *Phys. Chem. Chem. Phys.*, 2012, **14**, 8485–8497.
34 A. Michota and J. Bukowska, *J. Raman Spectrosc.*, 2003, **34**, 21–25.
35 C. J. Orendorff, A. Gole, T. K. Sau and C. J. Murphy, *Anal. Chem.*, 2005, **77**, 3261–3266.
36 R. H. Que, M. W. Shao, S. J. Zhuo, C. Y. Wen, S. D. Wang and S. T. Lee, *Adv. Funct. Mater.*, 2011, **21**, 3337–3343.
37 Q. Shao, R. H. Que, M. W. Shao, L. Cheng and S. T. Lee, *Adv. Funct. Mater.*, 2012, **22**, 2067–2070.
38 P. J. Schuck, D. P. Fromm, A. Sundaramurthy, G. S. Kino and W. E. Moerner, *Phys. Rev. Lett.*, 2005, **94**, 17402–17406.
39 V. Liberman, C. Yilmaz, T. M. Bloomstein, S. Somu, Y. Echegoyen, A. Busnaina, S. G. Cann, K. E. Krohn, M. F. Marchant and M. Rothschild, *Adv. Mater.*, 2010, **22**, 4298–4302.